Materials Today Bio 20 (2023) 100649

Contents lists available at ScienceDirect

Materials Today Bio

journal homepage: www.journals.elsevier.com/materials-today-bio

M2 macrophage-derived exosome-encapsulated microneedles with mild photothermal therapy for accelerated diabetic wound healing

Junkai Zeng [a,1], Zhenyu Sun [b,1], Feihui Zeng [c,1], Changjiang Gu [a], Xiongsheng Chen [a,d,*]

[a] Spine Center, Department of Orthopaedics, Changzheng Hospital, Naval Medical University (Second Military Medical University), Shanghai, 200003, PR China
[b] Department of Orthopaedics, Shanghai Sixth People's Hospital Affiliated to Shanghai Jiao Tong University School of Medicine, Shanghai, 200233, PR China
[c] Department of Endocrinology, Fujian Medical University Union Hospital, Fuzhou, 350001, PR China
[d] Department of Orthopaedics, Shanghai General Hospital, Shanghai Jiao tong University School of Medicine, Shanghai, PR China

ARTICLE INFO

Keywords:
Polydopamine
Exosomes
M2 macrophages
Hydrogel microneedle
Wound healing

ABSTRACT

Due to local overactive inflammatory response and impaired angiogenesis, current treatments for diabetic wounds remain unsatisfactory. M2 macrophage-derived exosomes (MEs) have shown considerable potential in biomedical applications, especially since they have anti-inflammatory properties that modulate macrophage phenotypes. However, exosome-based strategies still have limitations, such as short half-lives and instability. Herein, we develop a double-layer microneedle-based wound dressing system (MEs@PMN) by encapsulating MEs in the needle tips and polydopamine (PDA) nanoparticles in backing layer to simultaneously suppress inflammation and improve angiogenesis at the wound site. *In vitro*, released MEs increased macrophage polarization towards the M2 phenotype. In addition, mild heat (40 °C) generated by the photosensitive PMN backing layer contributed to improved angiogenesis. More importantly, MEs@PMN also showed promising effects in diabetic rats. The uncontrolled inflammatory response at the wound site was inhibited by MEs@PMN during a 14-day period; in addition, MEs and the photothermal effects produced by PMN provided a combined proangiogenic effect by improving the expression of CD31 and vWF. Collectively, this study provides a simple and efficient cell-free strategy for suppressing inflammation and promoting vascular regeneration to treat diabetic wounds.

1. Introduction

In the last five decades, the prevalence of diabetes has rapidly increased worldwide, showing an almost 10-fold increase [1]. Chronic refractory wounds are one of the most common complications of diabetes, and they cause a substantial burden to patients and health care systems [2]. Due to the impaired angiogenesis and chronic inflammation that occur in hyperglycaemic environments, the normal healing cascade is severely disrupted [3]. Currently, effective therapies for diabetic wounds remain elusive because of limited knowledge of the complex wound healing process. Thus, there is an urgent need to establish a multifunctional platform to not only regulate inflammation at the wound site but also promote revascularization and tissue regeneration.

Exosomes are extracellular vesicles released by various types of cells that regulate cell-to-cell communication by delivering their contents [4]. They have attracted worldwide attention due to their essential roles in health and diseases [5]. In addition, exosomes have exhibited superior biocompatibility, low immunogenicity and therapeutic targetability in many recently published studies, and as such, they have great potential for future applications in tissue regeneration [6,7]. Very recently, the therapeutic effects of exosomes have been verified in many tissues and organs, including the neurological, musculoskeletal, pulmonary and cardiovascular systems, in preclinical studies [8]. In addition, exosomes carry biomolecules including proteins, DNA, mRNAs and miRNAs, from the parent cells [9]. Therefore, they were endowed with biological advantages similar to those of their cells of origin. For example, M2 macrophages exhibit an anti-inflammatory phenotype and are involved in many inflammatory diseases including allergy, parasitic infection and tissue remodelling [10]. It has been reported that switching macrophage phenotypes at the wound site, specifically by stimulating M2 macrophage polarization, can inhibit apoptosis and inflammatory responses to facilitate wound healing [11]. Interestingly, M2 macrophage-derived

* Corresponding author. Spine Center, Department of Orthopaedics, Changzheng Hospital, Naval Medical University (Second Military Medical University), Shanghai, 200003, PR China. .
E-mail address: chenxiongsheng@vip.sohu.com (X. Chen).
[1] These authors contributed equally to this work.

https://doi.org/10.1016/j.mtbio.2023.100649
Received 28 February 2023; Received in revised form 13 April 2023; Accepted 28 April 2023
Available online 29 April 2023

exosomes (MEs) also target inflammation and show anti-inflammatory properties in inflammatory diseases [12]. Furthermore, in a previous study, MEs significantly promoted the switching of the macrophage phenotype from proinflammatory M1 phenotype to the anti--inflammatory M2 phenotype, thereby accelerating the healing of cutaneous wounds [13]. Considering the chronic and overactive inflammation at the diabetic wound site, MEs-loaded biomaterials might provide an effective strategy for promoting diabetic wound healing.

At present, exosome-based strategies still have limitations, such as a short half-lives and instability *in vivo* [14]. If free exosomes are injected directly at the wound site, it is difficult for them to remain at the site long enough to achieve satisfactory effects. Since the diabetic wound healing might require weeks, it is of great importance to design a stable and bioactive exosome delivery system to achieve prolonged therapeutic effects in the wound by inhibiting inflammation and improving angiogenesis. The progresses of tissue engineering have bridged the gap between engineering and medicine to advance healthcare treatment [15,16]. In recent years, a variety of novel materials, including organic, inorganic and hybrid dressings, have been studied to promote the desired biological response for the effective treatment of refractory wounds [17–19]. Among them, hydrogel hybrids are considered to be one of the most promising materials for tissue regeneration [20,21]. Currently, hydrogel microneedle (MN) patches fabricated by various techniques have attracted significant attention from researchers in the tissue-engineering field because of their superior biocompatibility, minimal invasiveness, extended drug retention time and high loading efficiency [22,23]. Specifically, bioactive components are encapsulated in the needle structure of MN which will be punctured into wound tissues. Compared with traditional drug delivery system, MN could release the encapsulated components in the deep layer of the dermis [24]. Stem cells, exosomes and other bioactive compounds have thus far been grafted onto MNs to develop minimally invasive treatments [25–27]. However, to the best of our knowledge, no previous study has prepared MEs-loaded MN patches and use them to accelerate wound repair. Therefore, it is urgently desired to develop a multifunctional delivery system to achieve the release of MEs, which could provide a potential therapeutic candidate for the treatment of diabetic wounds.

Inflammation, proliferation, and tissue remodelling are three main phases of the wound healing process [28]. Once the inflammation has subsided, revascularization is the main obstacle to successful diabetic wound healing. It is necessary to endow wound dressings with angiogenesis-promoting abilities. Metal ions, including Cu^{2+}, Zn^{2+} and Fe^{3+}, have been widely used in previous studies to promote angiogenesis [29]. However, the use of these ions may lead to high local concentrations at the wound side and toxic side effects [30]. Recently, a study suggested that MEs promoted angiogenesis by activating the Wnt signalling pathway [31]. Additionally, many papers have suggested that mild heat can promote the proliferation of human umbilical vein endothelial cells (HUVECs) to increase the density of newly born vessels in the granulation tissue. For example, inspired by hot springs, Sheng et al. designed a bioactive photothermal hydrogel (FA-NOCS) based on fayalite and N, O-carboxymethyl chitosan to promote angiogenesis for wound healing [32]. The mild photothermal effect (~40 °C) generated by FA-NOCS significantly upregulated angiogenesis-related gene and protein expression. Similarly, Xu et al. fabricated a novel photosensitive PDA/Cu hydrogel for wound healing. Under laser irradiation, the mild heat generated by this hydrogel successfully enhanced the expression of CD31 to promote angiogenesis *in vivo* [33]. Hence, we proposed to design a photosensitive MN patch to simultaneously achieve the sustained release of bioactive exosomes and mild photothermal effects to promote revascularization.

Based on the above considerations, we synthesized a multifunctional MEs@PMN platform for accelerating the healing of diabetic wounds (Scheme 1). MEs were isolated and encapsulated in needle tips, and could be released at the wound site to regulate inflammation and improve angiogenesis. Furthermore, polydopamine (PDA) -doped polyvinyl alcohol (PVA) solution was used as the backing layer of the MN patch (PMN). We hypothesize that the synergistic effect of MEs and mild photothermal effect generated by PDA under 808 nm laser irradiation would promote angiogenesis and granulation tissue formation. In this work, both *in vitro* and *in vivo* studies were performed to evaluate the effects of MEs@PMN on macrophage phenotype switching and

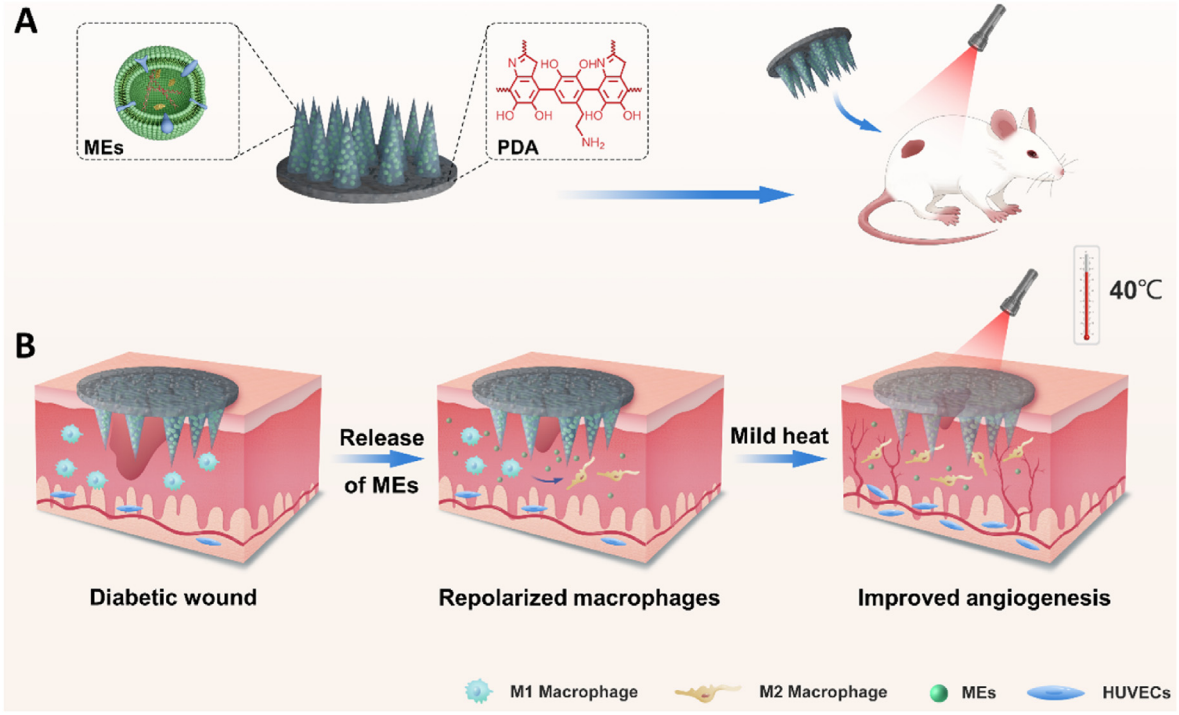

Scheme 1. (A) Schematic illustration of MEs@PMN for diabetic wound healing. (B) MEs@PMN for treating diabetic wound based on anti-inflammation and angiogenesis promotion.

angiogenesis, providing a promising candidate for diabetic wound healing.

2. Results and discussion

2.1. Characterization of MEs@PMN

The procedure of MEs@PMN preparation is presented in Fig. 1A. The MEs-HAMA prehydrogel and PDA-PVA solution were successively filled into mold. Subsequently, after UV- crosslinking and demoulding, the as-prepared MEs@PMN was stored in a dry environment for further use. The MEs were first characterized. As shown in Fig. 1B, TEM images revealed a typical cup-shaped morphology of MEs. NTA was then employed to measure the particle size distributions of the MEs (Fig. 1C). The diameters of the MEs ranged mainly from 70 to 200 nm, with the highest peak at approximately 100 nm. The expression of exosomal markers (TSG101 and CD9) in the MEs was further measured by western blotting (Fig. 1D). In addition, the negative marker calnexin was absent from lysates of M2 macrophages, but present in the MEs. As seen in digital images (Fig. 1E), the as-prepared MEs@PMN showed a disc-like shape (diameter 15 mm, height 2 mm). Due to the encapsulation of PDA nanoparticles, MEs@PMN exhibited a characteristic black appearance. As shown in Fig. 1F, a conical needle-like structure was observed by SEM. MNs were arranged orderly on the base of PDA-PVA, with a height of 300 μm and a base diameter of 100 μm. TEM images of PDA nanoparticles are also shown in Fig. 1G. PDA showed a uniform, circular shape with a diameter of approximately 100 nm. In addition, the surface morphology of PDA-PVA backing layer was also recorded by SEM. As shown in Fig. S1, original PVA backing layer showed a clear and clean appearance. As a comparison, PDA nanoparticles were homogeneously distributed on the surface of PDA-PVA. Furthermore, confocal laser scanning microscopy (CLSM) was used to observe the distribution of MEs. As shown in Fig. 1H, red fluorescence (Dil-labeled MEs) was evenly distributed in the needle structure of the MEs@PMN. The mean fluorescent intensity of Dil-labeled

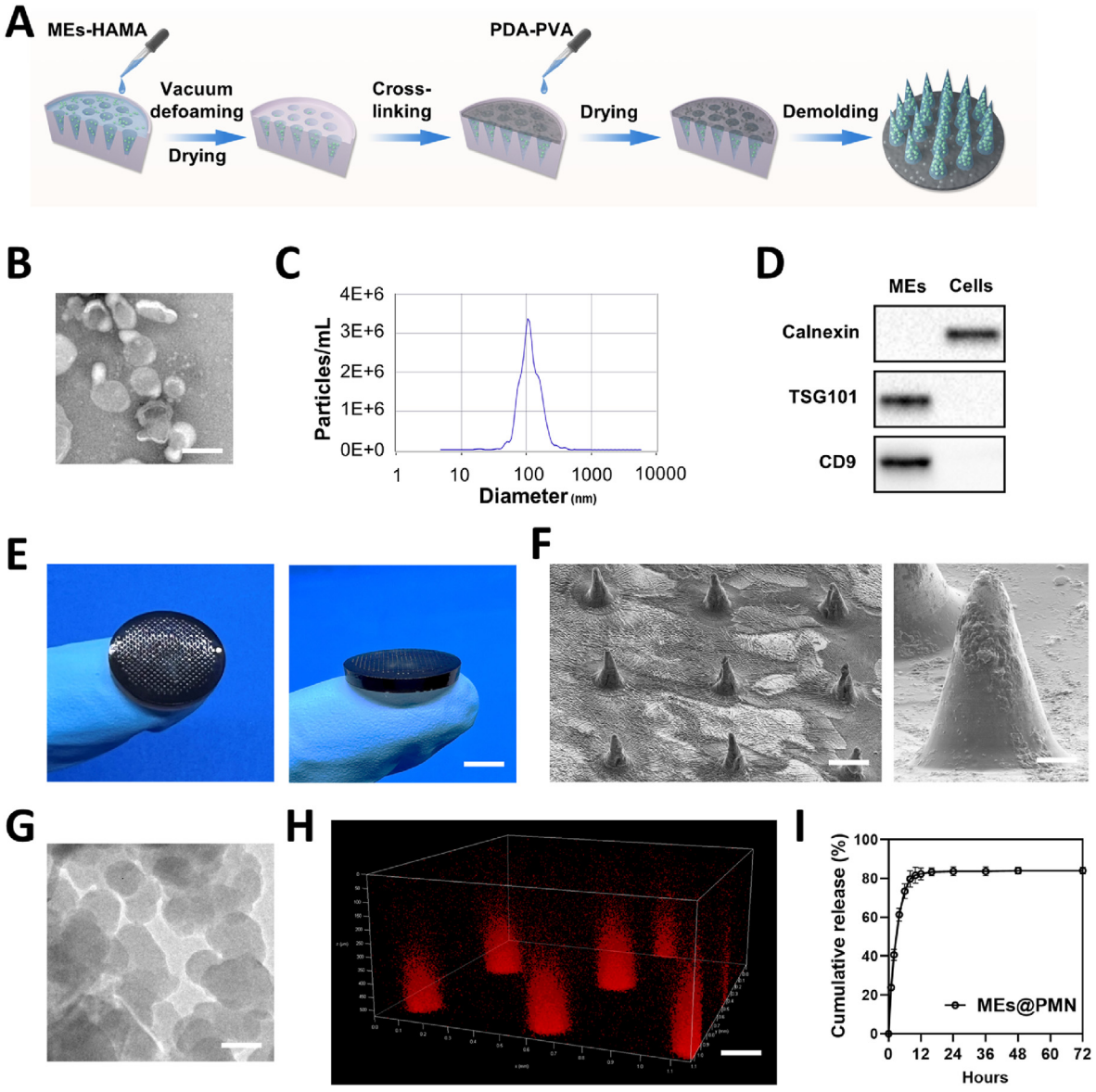

Fig. 1. Preparation and characterization of MEs@PMN. (A) Schematic diagram of MEs@PMN preparation process. (B) Representative TEM images of MEs. Scale bars, 100 nm. (C) Particle size distributions of MEs measured by NTA. (D) Exosomes markers (TSG101 and CD9) and negative marker (calnexin) were detected by western blot. (E) Digital images of MEs@PMN. Scale bars, 5 mm. (F) Representative SEM images of MEs@PMN. Scale bars, 150 μm & 25 μm. (G) Representative TEM images of PDA nanoparticles. Scale bars, 100 nm. (H) Dil staining of MEs encapsulated in MEs@PMN. Scale bars, 100 μm. (I) Cumulative release profile of MEs from the MEs@PMN within 72 h.

MEs was 148.23. Persistent inflammation at the wound site leads to abnormal levels of cytokines and apoptosis of cells, impairing the normal healing process [34]. Considering the importance of the anti-inflammatory effect of dressings for diabetic wounds, an *in vitro* ME release experiment was then performed. As indicated in Fig. 1I, the release curve indicated that the MEs were released rapidly at the initial stage, reaching 82.33 ± 3.06% release within 12 h. Then the release gradually stabilized, showing a final cumulative release rate of 84.00 ± 1.73% after 72 h.

2.2. Photothermal effect of MEs@PMN

As promising photothermal agents, PDA nanoparticles have been extensively studied in the context of hyperthermia in antibacterial and anticancer treatment due to their strong absorption in the visible and NIR regions and superior biocompatibility [35,36]. In the current study, PDA nanoparticles were encapsulated in the base of MEs@PMN to provide a mild photothermal effect for wound healing. The photothermal effects of the MEs@PMN functionalized with different concentrations (0, 25, 50, 75 and 150 μg ml^{-1}) of PDA nanoparticles were evaluated under 10-min NIR irradiation (1.0 W cm^{-2}). As seen in Fig. 2A&B, the rising rate of the temperature increased with the concentration of PDA nanoparticles. In addition, almost all the samples reached the peak surface temperatures within 120 s, and it was then maintained at a stable level. The peak temperatures of the MEs@PMN functionalized with different concentrations (0, 25, 50, 75 and 150 μg ml^{-1}) of PDA nanoparticles were determined to be 27.6 ± 0.1 °C, 31.0 ± 0.7 °C, 36.5 ± 1.8 °C, 39.9 ± 1.2 °C, and 47.0 ± 1.5 °C at an irradiation time point of 10 min, respectively (Fig. 2C). Considering the mild photothermal effect (~40 °C) has positive effect on angiogenesis, the concentration of 75 μg ml^{-1} was used for further study. The photostability of MEs@PMN (75 μg ml^{-1}) was also tested by 5 cycles of continuous NIR laser irradiation (1.0 W cm^{-2}). As shown in Fig. 2D, the photothermal effect of MEs@PMN did not significantly decay after five consecutive heating-cooling cycles, indicating the promising photothermal stability of the MEs@PMN. Furthermore, the UV–Vis absorption behaviours of the MEs@PMN and PDA-loaded MEs@PMN were measured by UV–vis spectroscopy (Fig. 2E). The encapsulation of PDA nanoparticles significantly improved the absorption intensity in the visible region across 400 nm–800 nm.

2.3. MEs@PMN promoted macrophage polarization toward the M2 phenotype

Macrophages are powerful immune effector cells that play important roles in defence against pathogens and maintaining homeostasis [37]. The biocompatibility of MEs@PMN on RAW264.7 macrophages was evaluated by CCK-8 assay. As shown in Fig. S2, RAW264.7 cells cultured with PMN and MEs@PMN both exhibited robust growth and viability during the 7-day period. Besides, no significant difference was found among the control, PMN and MEs@PMN, suggesting the promising biocompatibility of MEs@PMN. Two phenotypes of macrophages, alternatively activated and classically activated macrophages, are involved in the process of wound healing [25]. In diabetic wounds, an abnormal macrophage phenotype and uncontrolled inflammation result in abnormal physiological function. Excessive M1 macrophage numbers and deficient M2 macrophage numbers inhibit diabetic wound healing [38]. Therapies to reverse this trend could be applied to accelerate diabetic wound healing. Therefore, we investigated the effect of MEs@PMN on macrophage polarization in this section. The uptake of MEs released from MEs@PMN to RAW 264.7 macrophages was first studied in a cellular uptake experiment. As shown in Fig. 3A, diffuse red fluorescence could be found around the nuclei of macrophages, suggesting the successful uptake of MEs by RAW 264.7 cells. Second, flow cytometry was performed to quantitatively analyse macrophage polarization after

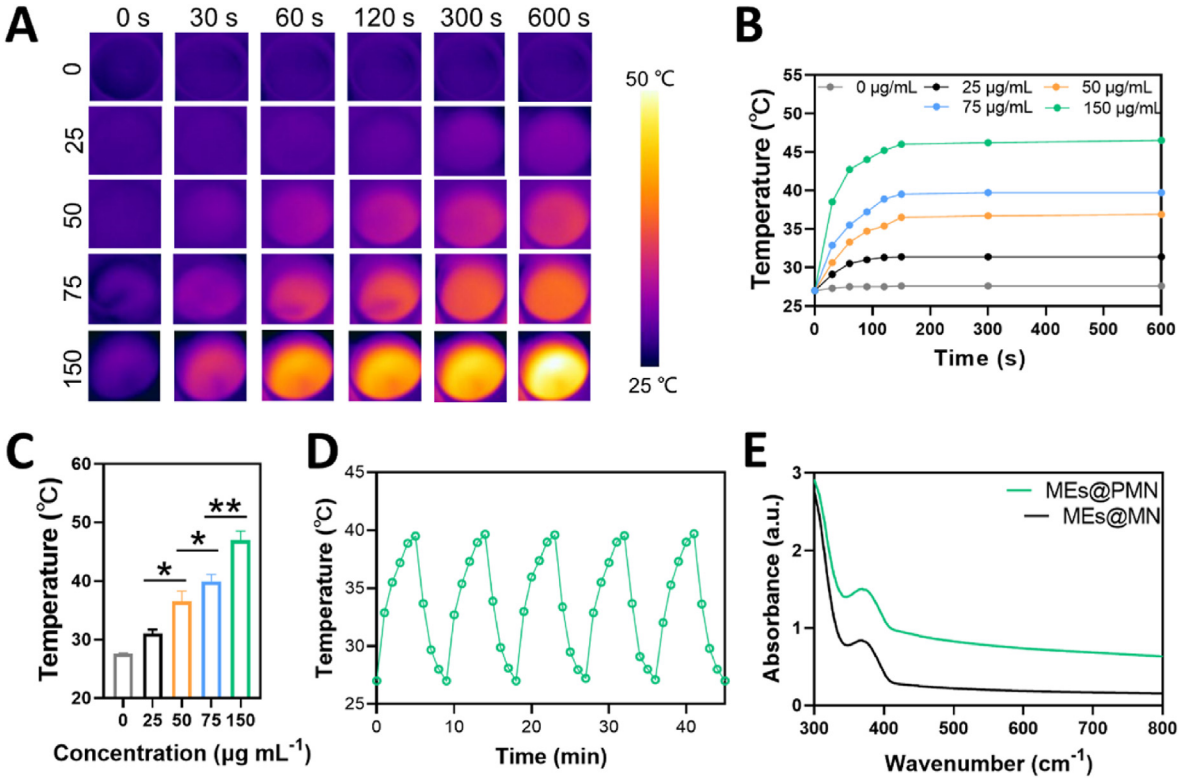

Fig. 2. Photothermal performance of MEs@PMN. (A) Infrared thermal images of MEs@PMN fabricated with different concentrations (0, 25, 50, 75 and 150 μg ml^{-1}) of PDA-PVA under NIR irradiation (1.0 W cm^{-2}). (B) Heating curves of various samples *in vitro*. (C) The maximum surface temperatures of different samples with 10-min NIR irradiation. (D) The photostability test of MEs@PMN fabicated with 75 μg ml^{-1} of PDA nanoparticles. (E) UV–Vis spectra. The experiments above were repeated three times.

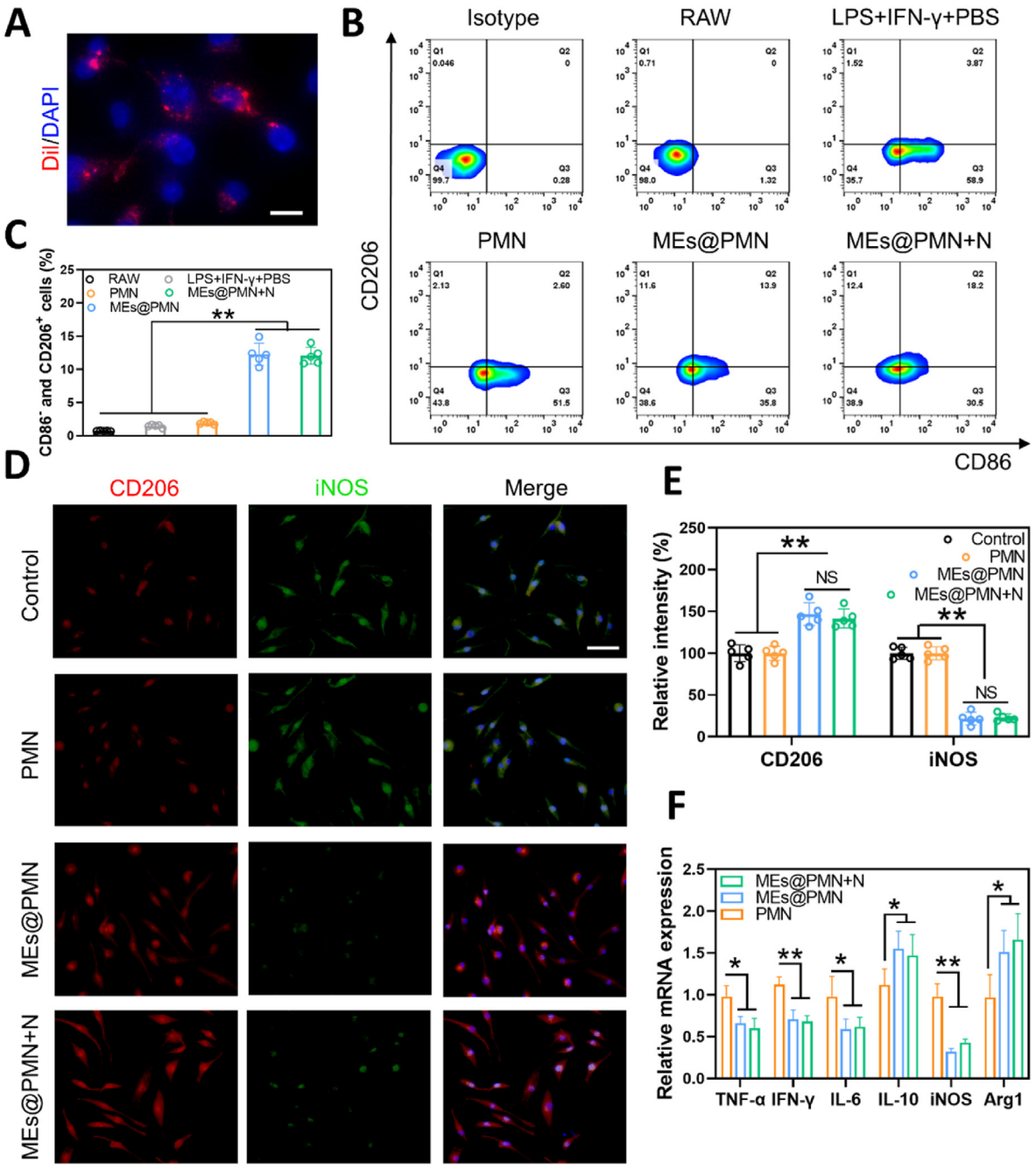

Fig. 3. Effect of MEs@PMN on polarization of macrophages. (A) Uptake of Dil-labeled MEs into RAW 264.7 macrophages. Scale bars, 20 μm. (B) Flowcytometry analysis of macrophages treated by MEs@PMN in the presence of LPS plus IFN-γ for 24 h. (C) Quantitative analysis of flowcytometry. (D) & (E) Representative images and quantitative analysis of CD206 (red) and iNOS (green) immunostaining. Scale bars, 100 μm *: $P < 0.05$, **: $P < 0.01$. (F) The result of qRT-PCR assay (TNF-α, IFN-γ, IL-6, IL-10, iNOS and Arg1). The experiments above were repeated five times. (For interpretation of the references to colour in this figure legend, the reader is referred to the Web version of this article.)

different stimulations. CD206 and CD86 were used as markers of M2 and M1 macrophages, respectively, for flow cytometry staining. To induce the M1 phenotype of macrophages, RAW264.7 cells were treated with LPS plus IFN-γ. Then PMN or MEs@PMN were used to stimulate M1 macrophages. Specifically, the effect of mild heat on macrophage polarization was also investigated. As indicated in Fig. 3B&C, the ratio of $CD206^+$ $CD86^-$ positive cells (M2 macrophages) was only $1.93 \pm 0.17\%$ in the LPS + IFN-γ+PBS group but sharply increased to $12.28 \pm 1.68\%$ in the MEs@PMN group and $12.04 \pm 1.26\%$ in the MEs@PMN + N group. This result suggested that MEs released from MEs@PMN significantly promoted macrophage polarization towards the M2 phenotype. In addition, the mild heat and a short period of NIR exposure (1 W cm^{-2}, 10 min) had no adverse impact on the polarization of macrophages. Third, immunostaining for iNOS and CD206 was performed *in vitro* (Fig. 3D). There was no obvious difference in the brightness and density of red and green fluorescence between the PMN and control groups. However, the use of MEs@PMN greatly improved the density of red fluorescence while decreasing the density of green fluorescence, indicating that MEs@PMN induced a conversion of the M1 to M2 phenotype *in vitro*. In addition, no significant difference was found between MEs@PMN and MEs@PMN + N according to the analysis in Fig. 3E, which was consistent with the flow cytometry results. Finally, the

expression of proinflammatory and anti-inflammatory genes was measured by qRT–PCR (Fig. 3F). In comparison to the control, MEs@PMN markedly upregulated the expression of Arg1 and IL-10, demonstrating the anti-inflammatory effect. Furthermore, MEs@PMN significantly downregulated the expression of TNF-α, IFN-γ, IL-6 and iNOS, suggesting an inhibitory effect on M1-phenotype polarization. Overall, these results indicated that MEs@PMN regulated inflammation *in vitro* by repolarizing M1 proinflammatory macrophages towards the anti-inflammatory M2 phenotype. It could also be concluded that mild heat generated by MEs@PMN had no significant effect on macrophage polarization.

2.4. MEs@PMN with mild heat promoted angiogenesis in vitro

Bioactive contents of exosomes enable them to regulate tissue regeneration. Emerging evidence has suggested that exosomes play an

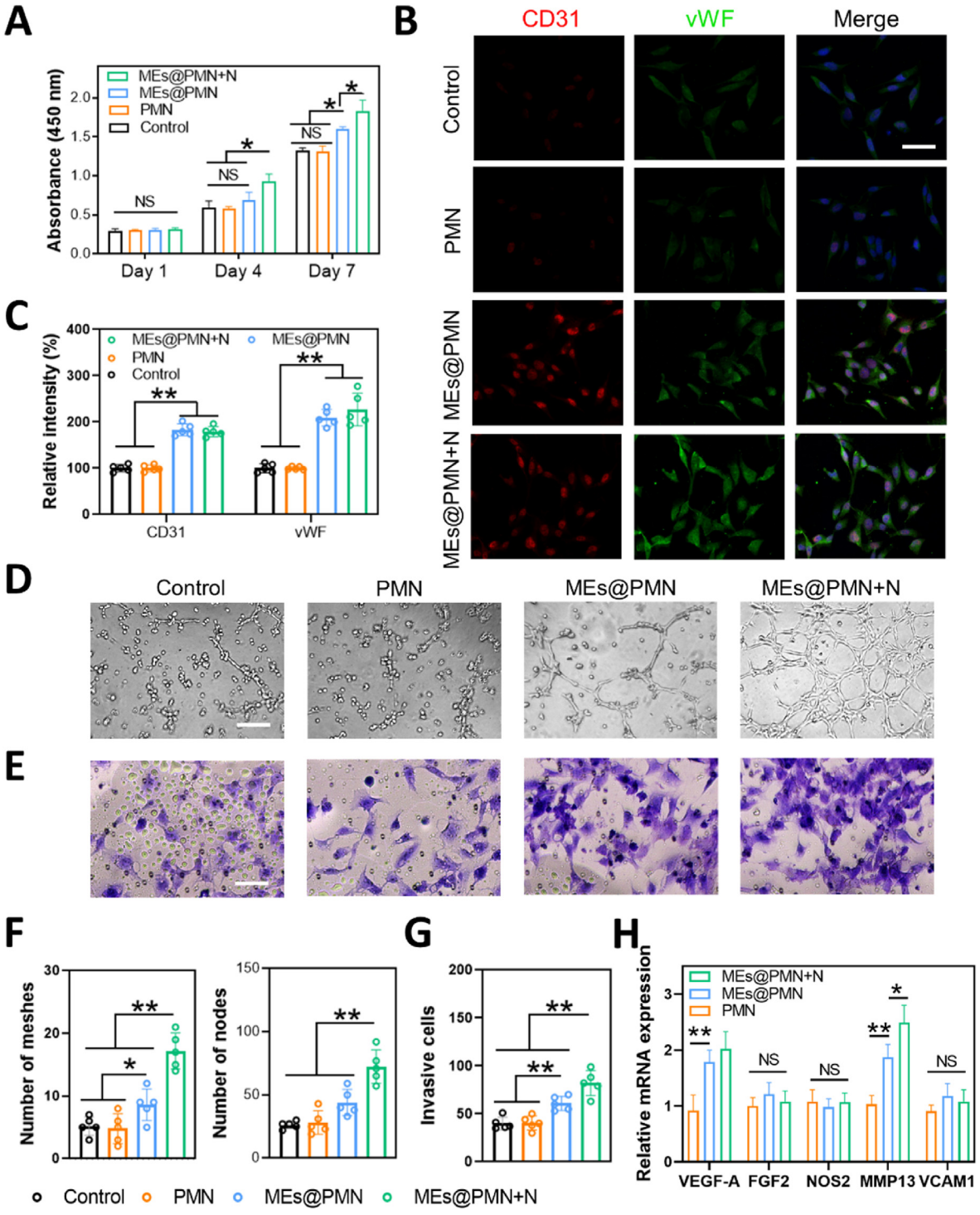

Fig. 4. The effect of MEs@PMN with mild heat on angiogenesis *in vitro*. (A) CCK-8 assay of HUVECs. (B) Immunofluorescence staining of vWF and CD31 in HUVECs. Scale bars, 50 μm. (C) Quantitative analysis of immunofluorescence staining. (D) Representative images of the tube formation assay. Scale bars, 50 μm. (E) Representative images of the Transwell assay. Scale bars, 50 μm. (F) Quantitative analysis of the tube formation assay. (G) Quantitative analysis of the Transwell assay. (H) The result of qRT-PCR assay (VEGF-A, FGF2, NOS2, MMP13 and VCAM1). The experiments above were repeated five times.

essential role in angiogenesis [39,40]. MEs have also shown potential in promoting revascularization. For example, Huang et al. revealed that MEs improved angiogenesis after spinal cord injury (SCI) by enhancing the expression of pro-angiogenesis factors (HIF-1α and VEGF) [41]. Similarly, another study showed that MEs stimulated the angiogenic activities of microvascular endothelial cells *in vitro*, thereby promoting revascularization after SCI [31]. Inspired by these studies, MEs were loaded in PMN in the current study to improve angiogenesis at the wound site. In this section, the angiogenic effect of MEs@PMN was evaluated by a series of assays. First, the CCK-8 assay was conducted to evaluate the growth of HUVECs after various treatments. As shown in Fig. 4A, MEs@PMN slightly increased the proliferation of HUVECs at Days 4 and 7. Furthermore, mild heat generated by MEs@PMN with NIR irradiation significantly promoted the growth of HUVECs. Second, immunostaining for CD31 and vWF was performed *in vitro* (Fig. 4B). Compared with the control and PMN, the brightness and density of red (CD31)/green (vWF) fluorescence signatures were sharply increased after MEs@PMN, indicating that the released MEs upregulated the expression levels of CD31 and vWF. According to the quantitative analysis in Fig. 4C, the expression of vWF was enhanced by MEs@PMN + N in comparison to MEs@PMN without mild heat; however, no significant difference was found. Third, the angiogenic effect of MEs@PMN was studied by a tube formation assay. The proangiogenic effect of mild heat is shown in Fig. 4D&F. After 6 h of incubation, many capillary-like structures could be observed in the MEs@PMN + N group, with a considerable increase in the number of formed meshes and nodes in comparison to the group without light irradiation. In addition, MEs@PMN + N was found to promote the cell migration of HUVECs (Fig. 4E&G). The qRT–PCR results suggested that MEs@PMN with or without light irradiation significantly upregulated the expression of VEGF-A and MMP13 (VEGF-A: 0.92-fold in PMN, 1.79-fold in MEs@PMN, 1.92-fold in MEs@PMN + N; MMP13: 1.03-fold in PMN, 1.97-fold in MEs@PMN, 2.39-fold in MEs@PMN + N). The angiogenic effect of mild heat was also proven by several publications. A previous study found that elevated core temperatures maintained at 41.5–42.5 °C for 15 min promoted the growth of new blood vessels [42]. Similarly, Guo et al. also proved that mild hyperthermia upregulated VEGF expression, resulting in accelerated angiogenesis [43]. Overall, our study proved that MEs released from MEs@PMN and mild heat generated by NIR irradiation contributed greatly to angiogenesis *in vitro*.

2.5. MEs@PMN with mild heat accelerated diabetic wound healing in vivo

In vitro experiments have demonstrated the promising anti-inflammatory and proangiogenic potential of MEs@PMN. We investigated the wound healing efficiency of MEs@PMN with mild heat *in vivo* using a rat model of diabetic wounds. A schematic diagram of the *in vivo* study is presented in Fig. 5A. In the MEs@PMN + N group, the temperatures at the wound site of the rats were increased from the basal temperature of 37 °C to approximately 40.0 °C under NIR light irradiation, and then the temperatures were maintained at 39.5–40.5 °C for 15 min on Days 1, 3 and 5. Representative images of diabetic wounds after various treatments at different treatment times are shown in Fig. 5B. In comparison to the control, the use of PMN only slightly decreased the wound area at Day 14. With the release of MEs from MEs@PMN + N, the wound size was significantly reduced. Furthermore, mild heat also exhibited a positive effect on wound healing. Compared with the MEs@PMN group, the MEs@PMN + N group showed a faster rate of wound healing starting on Day 5. At the end point, the wound areas of the MEs@PMN and the MEs@PMN + N were 17.43% and 5.01%, respectively. The histological structures of wound tissues after different treatments were also evaluated by H&E and Masson's trichrome staining. As shown in Fig. 5D, large residual scars and numerous inflammatory cells were found in the control and PMN groups. In comparison, MEs@PMN and MEs@PMN + N had mild inflammation. The quantitative analysis of inflammatory cells after various treatments in Fig. 5F demonstrated that inflammatory cells significantly decreased with MEs@PMN or MEs@PMN + N application, proving the anti-inflammatory effect of released MEs. More importantly, an almost complete epidermal layer was observed in the MEs@PMN + N group. Masson's trichrome staining was also conducted to study collagen deposition at the wound site (Fig. 5E). The results showed a larger area of collagen fibres in the MEs@PMN + N group than in the other groups. According to the quantitative analysis in Fig. 5F, the percentages of collagen deposition area were 24.03%, 31.57%, 49.93% and 63.83% in the control, PMN, MEs@PMN and MEs@PMN + N groups, respectively. The structure and functions of MEs@PMN both play important roles in animal experiment. There are mainly two advantages of the special structure of MEs@PMN. Firstly, the needle tips could bypass the barrier of skin to deliver bioactive components in the deep layer of the dermis. Secondly, MEs@PMN served as a physical barrier to protect the wound from the external environment. Besides, the functions of MEs@PMN and mild heat also contributed to accelerated healing of diabetic wounds by suppressing inflammation and improving collagen deposition.

2.6. MEs@PMN with mild heat inhibited inflammation and promoted angiogenesis in vivo

To investigate the mechanisms by which MEs@PMN with mild heat promotes diabetic wound healing *in vivo*, immunofluorescence staining of wound tissues was performed. The prolonged inflammatory phase is the main challenge for the treatment of diabetic wounds. The results of H&E staining suggested that MEs released from MEs@PMN suppressed inflammation at the wound site. Combined with the encouraging results *in vitro* that MEs@PMN promoted macrophages towards the M2 phenotype, we then studied the effect of MEs@PMN on the polarization status of macrophages in diabetic wounds. First, immunostaining for TNF-α was performed to evaluate the inflammation status of wound tissues. As shown in Fig. 6A&E, in comparison to the control and PMN groups, the density and intensity of red fluorescence signatures drastically decreased in the MEs@PMN-treated groups, indicating much milder inflammation. Then, immunostaining of iNOS and CD206 was conducted to label M1 and M2 macrophages, respectively. Consistent with the *in vitro* results, the ratio of M1 macrophages dramatically declined, while the ratio of M2 macrophages increased after MEs@PMN application (Fig. 6B&C), demonstrating the shifting of macrophages from the M1 phenotype to a proregenerative M2 phenotype. In addition, no significant difference was found between the MEs@PMN and MEs@PMN + N groups according to the quantitative analysis in Fig. 6F&G, confirming that mild heat generated by NIR irradiation had no significant effect on macrophage polarization in diabetic wounds. Furthermore, Fig. 6D shows the results of immunofluorescence staining for vascular endothelial-specific markers, including CD31 (red) and vWF (green). Both green and red fluorescence were greatly enhanced after MEs@PMN application, proving the pro-angiogenic effect of MEs. In addition, a significantly higher expression of CD31 was found in MEs@PMN + N (Fig. 6I), which may explain the accelerated wound healing in comparison to MEs@PMN without NIR irradiation. Overall, immunostaining of wound tissues further confirmed the beneficial effects of MEs@PMN + N in modulating the inflammatory microenvironment and promoting angiogenesis.

2.7. Evaluation of biosafety

At the endpoint of the experiment, major organs, including the heart, liver, spleen, lung, and kidney, were harvested from diabetic rats in the control and MEs@PMN + N groups to evaluate the biosafety of this novel therapy (Fig. S3). No obvious microscopic difference in these organs was found between control and MEs@PMN + N groups. In addition, the hepatic and renal functions of rats treated with MEs@PMN + N were also within the normal range (Fig. S4). The above results suggested that MEs@PMN + N treatment was not toxic to diabetic rats.

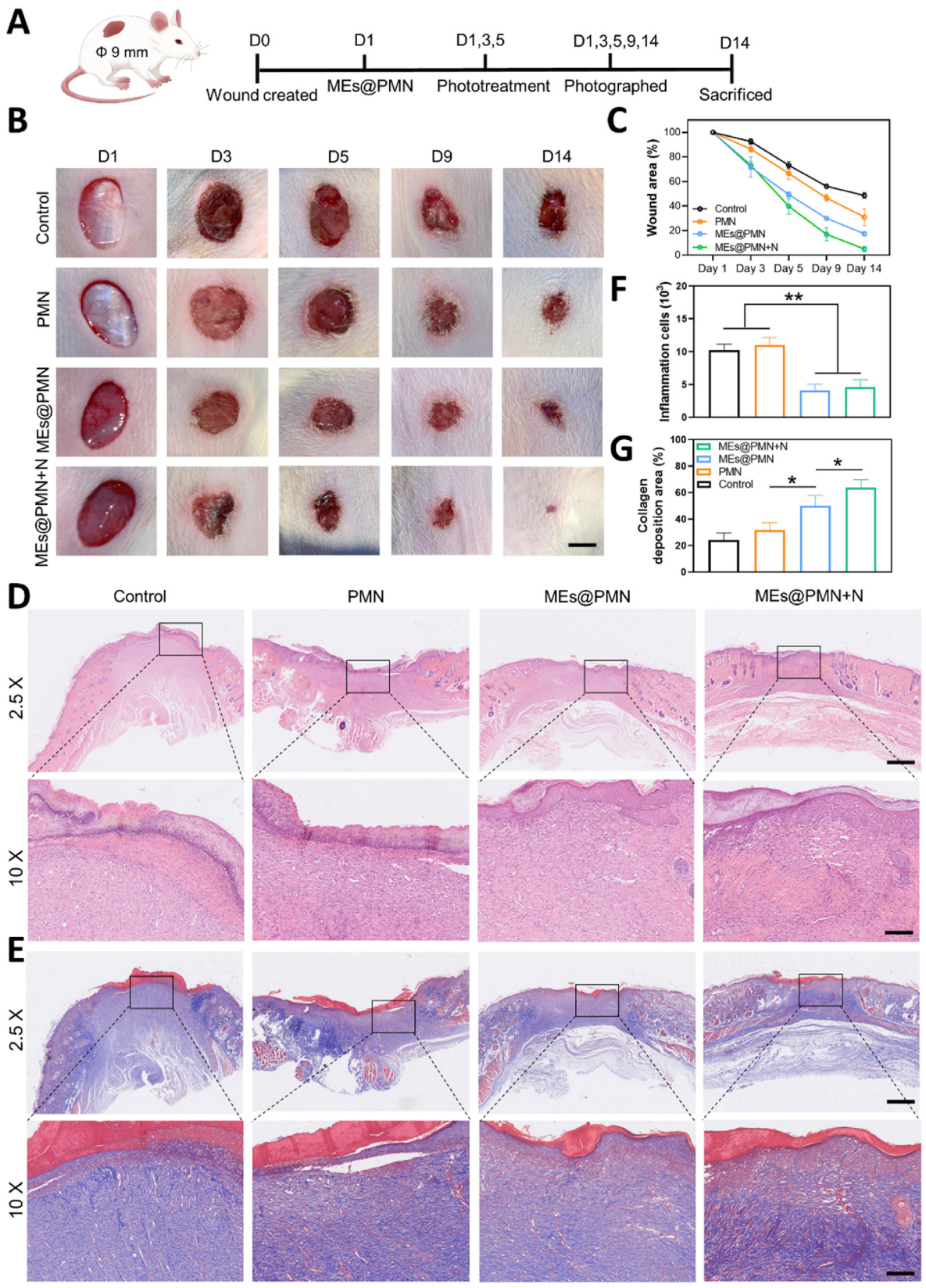

Fig. 5. *In vivo* evaluation of MEs@PMN for diabetic wounds. (A) Schematic diagram of the animal experiment. (B) Photographs of diabetic wounds after various treatments at different treatment time. Scale bars, 2.5 mm. (C) Recording of wound area durinng the 14-day period. (D) Representatve images of H&E stainings. Scale bars, 2.5 mm & 600 μm. (E) Representative images of Masson's trichrome stainings. Scale bars, 2 mm & 600 μm. (F) Quantitative analysis of H&E stainings: counting of inflammation cells. (G) Quantitative analysis of Masson's trichrome stainings: percentages of collagen deposition area. The experiments above were repeated three times.

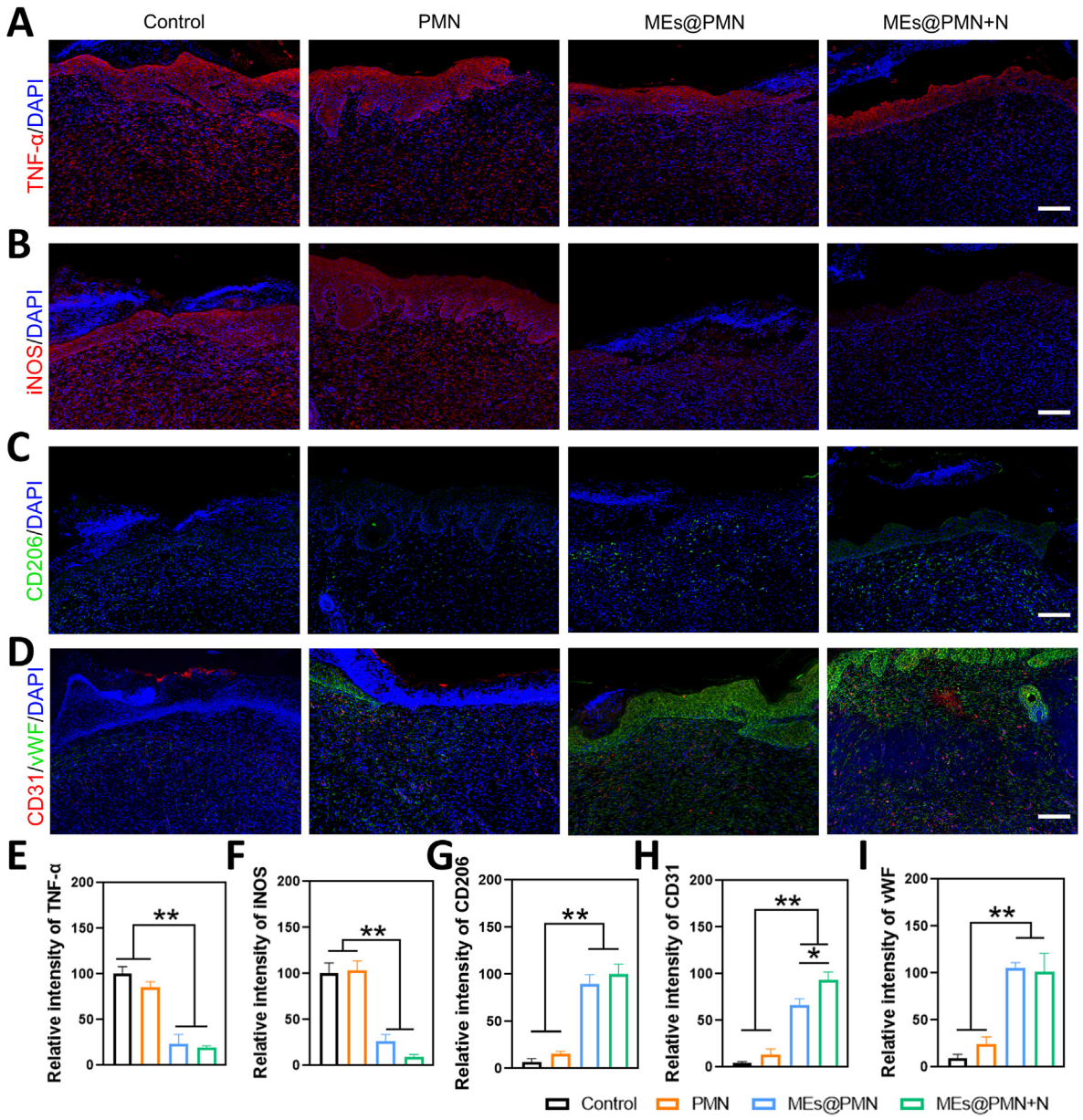

Fig. 6. *In vivo* evaluation of anti-inflammation and pro-angiogenic effects of various treastments. (A) Representatve images of TNF-α immunostaining. Scale bars, 100 μm. (B) Representatve images of iNOS immunostaining. Scale bars, 100 μm. (C) Representatve images of CD206 immunostaining. Scale bars, 100 μm. (D) Representatve images of CD31 and vWF immunostainings. Scale bars, 100 μm. (E ~ I) Quantitative analysis of immunostainings. The experiments above were repeated three times.

3. Conclusions

Using both *in vitro* and *in vivo* experiments, we have shown that exosome-loaded photosensitive hydrogel microneedles (MEs@PMN) accelerated diabetic wound healing by suppressing inflammation and promoting angiogenesis. MEs@PMN hydrogel system exhibited superior biocompatibility and considerable photothermal effects. Released MEs significantly promoted the transition of the macrophage phenotype from the proinflammatory M1 phenotype to the anti-inflammatory M2 phenotype, and they also demonstrated proangiogenic effects at the wound site. Notably, we confirmed that mild heat at approximately 40 °C had positive effects on angiogenesis. Taken together, the current study describes a promising cell-free approach for suppressing inflammation and promoting revascularization to accelerate diabetic wound healing.

4. Materials and methods

4.1. Materials

Methacrylated hyaluronic acid hydrogel (HAMA), polyvinyl alcohol (PVA) and lithium phenyl-2,4,6-trimethylbenzoylphosphinate (LAP) were bought from Engineering for Life (Suzhou, China). Tris (hydroxymethyl)-aminomethane hydrochloride and dopamine hydrochloride were bought from Aladdin Industrial Corporation. Dil was bought from Beyotime (China). All other chemical reagents were obtained from Sigma-Aldrich (USA).

4.2. Exosomes isolation and identification

RAW264.7 cells were purchased from Procell Life Science & Technology (China) and cultured in DMEM supplemented with 10% FBS and

1% mixture of penicillin-streptomycin at 37 °C with 5% CO_2. To induce the M2 phenotype, RAW264.7 monocyte macrophages were treated with IL-4 (100 ng/ml) in serum-free medium for 24 h. Then the ultracentrifugation method was performed to isolate MEs. Briefly, after M2 macrophages reached 80%–90% confluence, the supernatants were collected and centrifugated at 300 g for 15 min to remove cell pellet firstly. Then dead cells and debris were removed by a centrifugation at 10,000*g* for 15 min. The resultant supernatant was transferred to ultracentrifuge tubes (Beckman, USA) and centrifuged at 100,000 g for 3 h to collect MEs. Finally, MEs were suspended with PBS and stored in −80 °C before further use. To characterize the isolated exosomes, TEM (Tecnai Spirit, FEI, USA) was employed to observe the morphology of MEs. Additionally, NTA (ZetaView PMX 110, Particle Metrix, German) was used to measure the zeta potentials and sizes of MEs. And the exosomes markers of MEs were determined by western blotting.

4.3. Preparation of MEs@PMN

To prepare the MEs-HAMA pre-hydrogel, the MEs (100 μg/ml) were added into the HAMA solution (5% w/v) with a LAP solution (0.25% w/v) and dispersed evenly using ultrasound for 5 min. To prepare the PDA-PVA solution, PDA nanoparticles (75 μg/ml) were added into the PVA solution (20% w/v) and dispersed evenly by magnetic stirring for 30 min. Then MEs-HAMA pre-hydrogel solution (300 μL) was filled into a polydimethylsiloxane (PDMS) mold. After centrifugation and vacuum debubbling, MEs-HAMA was dried at 30 °C for 6 h. The MEs@PMN was then solidified by 60s of 405 nm UV irradiation. Thereafter, the PDA-PVA solution (300 μL) was added to cover the tips, and dried at 35 °C for 16 h. Finally, MEs@PMN was demolded from the PDMS mold and stored under dry conditions at 4 °C before further use.

4.4. Characterizations of MEs@PMN

The surface morphology of PVA, PDA-PVA and MEs@PMN was observed by SEM (Hitachi, S-4800, Japan). The morphology of PDA nanoparticles was viewed by TEM (Tecnai Spirit, FEI, USA). The UV–Vis absorption spectra of MEs@PMN were determined using a UV–vis spectrophotometer (UV-3600, Shimadzu, Japan).

4.5. Photothermal properties of MEs@PMN

MEs@PMN samples fabricated with different concentrations of PDA nanoparticles (0, 25, 50, 75 and 150 μg ml^{-1}) were immersed in 1 ml PBS solution firstly, and then received a 10-min irradiation by 808 nm laser. An infrared thermograph (FLIR E50 instrument, FLIR Systems, USA) was used to record the temperature changes and IR thermal images. In addition, to test the photostability of MEs@PMN, samples were irradiated using 808 nm laser (1.0 W cm^{-2}, 10 min) for five cycles.

4.6. Evaluation of MEs distribution in PMN

Isolated MEs were firstly stained by DiI solution (2 mg·mL-1, Beyotime, China). Then excess dye was removed by ultracentrifugation at 100,000 g for 70 min at 4 °C. After successful encapsulation of labeled MEs in PMN patches, the distribution of MEs was observed by a confocal laser scanning microscopy (CLSM, TCS SP8, Leica, Germany). And the fluorescence quantitative analysis was performed with ImageJ.

4.7. In vitro release of MEs

To study the release behavior of the MEs from MN patch, MEs@PMN scaffolds were fabricated and then washed with PBS to remove the unconjugated MEs. Firstly, MEs@PMN patches were immersed in 1 ml PBS in a 24-well plate (Corning, USA) in a 37 °C incubator. At different points of time (1, 2, 4, 6, 8, 10, 12, 16, 24, 36, 48, 72 h), the solution in the 24-well plate was collected and replaced by the same volume of fresh PBS. The concentration of MEs in the collected medium was detected by the BCA kit (Beyotime, China). The release rate of MEs was calculated by the following formula:

$$C = B/A \times 100\%$$

where C is the release rate, B refers to the cumulative amount of MEs in the collected medium; A refers to the total amount of MEs (30 μg) in a MEs@PMN.

4.8. Biocompatibility evaluation of MEs@PMN

CCK-8 assay was performed to assess the biocompatibility of MEs@PMN on RAW264.7 cells during the 7-day period. Briefly, RAW264.7 cells were cultured with various samples. At day 1, 4 and 7, CCK-8 diluent (Dojindo, Japan) was added to each well to a final concentration of 10% (v/v). Subsequently, the resultant mixture was incubated at 37 °C for 2 h, and then the OD450 value was measured.

4.9. Evaluation of macrophage repolarization

First, RAW264.7 macrophages were firstly induced to proinflammatory M1 phenotype by culturing with 100 ng/ml LPS and 20 ng/ml IFN-γ for 24 h. Second, M1 phenotype macrophages were co-cultured with MEs@PMN or PMN in a transwell system. In brief, MEs@PMN or PMN was immersed in culture medium in the upper chamber of a 24-well transwell plate (Corning, USA), while M1 phenotype macrophages were seeded in the lower chamber. For MEs@PMN + N group, samples were irradiated with 808 nm laser (1 W cm^{-2}) for 10 min to evaluate the side effect of laser irradiation on the macrophage polarization. Immunofluorescence staining for CD206 (red) and iNOS (green) was performed to evaluate the effect of MEs@PMN on macrophage repolarization. The results of flow cytometry were analyzed using a flow cytometer (CyAN ADP, Beckman, USA). CD206-negative and CD86-positive cells were identified as M1 macrophages, while CD86-negative and CD206-positive cells were identified as M2 macrophages. SIX groups were set: isotype, raw, PBS (Control), PMN, MEs@PMN and MEs@PMN + N. The expression of M1 macrophages related genes including IL-6, TNF-α, IL-1β and iNOS were also evaluated by qRT-PCR and the results were calculated by the $2^{-\Delta\Delta Ct}$ method. Primer sequences used in this study are presented in Table S.

4.10. Evaluation of angiogenesis

The effect of different treatments on angiogenesis were evaluated using HUVECs bought from Procell Life Science & Technology (China). Four groups were set: Control, PMN, MEs@PMN and MEs@PMN + N. For MEs@PMN + N group, samples received a 10-min 808 nm laser (1 W cm^{-2}) irradiation. First, CCK-8 analysis was performed to study the cell viability of HUVECs during the 7-day period. Subsequently, immunofluorescence of vWF (green) and CD31 (red) were performed to evaluate the effect of MEs@PMN on angiogenesis. In addition, tube formation assay was conducted as previously described [44]. The newly-formed meshes and nodes were counted under light microscopy, respectively. The migration of HUVECs was evaluated using the transwell assay as previously described [45]. Briefly, PMN or MEs@PMN was placed on the lower chamber of a 24-well transwell plate (Corning, USA), while HUVECs were seeded in the upper chamber. After 48 h co-culture, migrated HUVECs were fixed by 4% paraformaldehyde and stained by 0.5% crystal violet (Beyotime, China), then observed using a light microscope. In addition, the expressions of angiogenic genes including VEGFR-A, FGF2, NOS2, MMP13 and VCAM1 were also evaluated by qRT-PCR and the results were calculated by the $2^{-\Delta\Delta Ct}$ method. Primer sequences used in this study are presented in **Table S**1.

4.11. Animal model of diabetic wound

The animal experiments were performed under the authorization of the Animal Committee of Naval Medical University (Shanghai, China). Eight-week-old female Sprague Dawley rats purchased from Shanghai Institute for Family Planning were induced to diabetes by a single intraperitoneal injection of streptozotocin (90 mg/kg). The glucose of rats was measured twice a week and rats with stable high blood glucose levels (300 mg/dl) for two weeks were used in the following experiments. Diabetic rats were randomly divided into four groups: Control, PMN, MEs@PMN and MEs@PMN + N. In brief, rats were anesthetized by isoflurane gas firstly. Then all rats were shaved and sterilized, and two round full-thickness skin defects with a diameter of 9 mm were created with on the back of each rat. For the MEs@PMN + N group, the wounds received 10-min 808 nm NIR laser (1 W cm^{-2}) irradiations at Days 1, 3, and 5. The temperature changes of wounds with different dressings under laser irradiation were recorded by an infrared thermograph (FLIR E50 instrument, FLIR Systems, USA). Photographs of the wounds were taken at Days 1, 3, 5, 9 and 14. To calculate the wound area, MEs@PMN was carefully removed before the photograph was taken. The wound area was measured by Image J (1.52q, National Institutes of Health, USA).

4.12. Histological analysis and immunofluorescence labelling

At Day 14, all rats were euthanized, the wound tissues were harvested and fixed by 4% paraformaldehyde. Then the tissues were embedded in paraffin and sectioned at 5 μm intervals. H&E staining and Masson's trichrome staining were performed to study the re-epithelialization and collagen deposition of wounds treated by various methods. TNF-α immunostaining was used to evaluate the inflammation status of wound tissues. Furthermore, immunofluorescence staining for CD206 (green) and iNOS (red) was performed to evaluate the angiogenesis at the wound site. In addition, immunofluorescence staining for CD31 (red) and vWF (green) was used to measure the angiogenesis at the wound site.

4.13. Biosafety evaluation

Major organs of diabetic rats treated with MEs@PMN, including the heart, liver, spleen, lung and kidney, were harvested carefully and then fixed by 4% paraformaldehyde. Subsequently, H&E staining was performed to analyse their microstructures. In addition, blood samples of experimental rats were collected and biochemical analyses were performed to analyse the liver and renal functions.

4.14. Statistical analysis

All experimental data are presented as mean ± standard deviation (SD). The difference between groups was evaluate d by multiple t tests or two-way ANOVA. A value of $p < 0.05$ was considered statistically significant for all comparisons. * indicates $p < 0.05$, ** indicates $p < 0.01$.

Credit author statement

Junkai Zeng: Conceptualization, Investigation, Writing- Original draft preparation. **Zhenyu Sun:** Investigation, Validation. **Feihui Zeng:** Conceptualization, Writing- Reviewing and Editing. **Changjiang Gu**: Investigation, Validation. **Xiongsheng Chen**: Writing- Reviewing and Editing, Supervision, Funding acquisition.

Declaration of competing interest

The authors declare that they have no known competing financial interests or personal relationships that could have appeared to influence the work reported in this paper.

Data availability

Data will be made available on request.

Acknowledgements

J. Zeng, Z. Sun and F. Zeng contributed equally to this work. We gratefully acknowledge the financial support from the National Natural Science Foundation of China (82172472).

Appendix A. Supplementary data

Supplementary data to this article can be found online at https://doi.org/10.1016/j.mtbio.2023.100649.

References

[1] A. Sonmez, C. Haymana, I. Demirci, M. Cesur, M. Rizzo, I. Tasci, Critical questions in diabetes management: what are the most compelling challenges and how can we handle them? Int J Cardiol Cardiovasc Risk Prev 15 (2022), 200160 https://doi.org/10.1016/j.ijcrp.2022.200160.
[2] J. Ouyang, X. Ji, X. Zhang, C. Feng, Z. Tang, N. Kong, A. Xie, J. Wang, X. Sui, L. Deng, Y. Liu, J.S. Kim, Y. Cao, W. Tao, In situ sprayed NIR-responsive, analgesic black phosphorus-based gel for diabetic ulcer treatment, Proc. Natl. Acad. Sci. U. S. A. 117 (46) (2020) 28667–28677, https://doi.org/10.1073/pnas.2016268117.
[3] L.M. Morton, T.J. Phillips, Wound healing and treating wounds: differential diagnosis and evaluation of chronic wounds, J. Am. Acad. Dermatol. 74 (4) (2016) 589–605, https://doi.org/10.1016/j.jaad.2015.08.068, quiz 605-6.
[4] R. Kalluri, V.S. LeBleu, The biology, function, and biomedical applications of exosomes, Science 367 (6478) (2020), https://doi.org/10.1126/science.aau6977.
[5] H. Yu, Y. Huang, L. Yang, Research progress in the use of mesenchymal stem cells and their derived exosomes in the treatment of osteoarthritis, Ageing Res. Rev. 80 (2022), 101684, https://doi.org/10.1016/j.arr.2022.101684.
[6] X.C. Jiang, T. Zhang, J.Q. Gao, The in vivo fate and targeting engineering of crossover vesicle-based gene delivery system, Adv. Drug Deliv. Rev. 187 (2022), 114324, https://doi.org/10.1016/j.addr.2022.114324.
[7] L. Yang, K.D. Patel, C. Rathnam, R. Thangam, Y. Hou, H. Kang, K.B. Lee, Harnessing the therapeutic potential of extracellular vesicles for biomedical applications using multifunctional magnetic nanomaterials, Small 18 (13) (2022), e2104783, https://doi.org/10.1002/smll.202104783.
[8] M. Brennan, P. Layrolle, D.J. Mooney, Biomaterials functionalized with MSC secreted extracellular vesicles and soluble factors for tissue regeneration, Adv. Funct. Mater. 30 (37) (2020), https://doi.org/10.1002/adfm.201909125.
[9] M. Javadi, J.S. Rad, M.S.G. Farashah, L. Roshangar, An insight on the role of altered function and expression of exosomes and MicroRNAs in female reproductive diseases, Reprod. Sci. 29 (5) (2022) 1395–1407, https://doi.org/10.1007/s43032-021-00556-9.
[10] R.A. Villarreal-Leal, G.D. Healey, B. Corradetti, Biomimetic immunomodulation strategies for effective tissue repair and restoration, Adv. Drug Deliv. Rev. 179 (2021), 113913, https://doi.org/10.1016/j.addr.2021.113913.
[11] J.C. Gensel, B. Zhang, Macrophage activation and its role in repair and pathology after spinal cord injury, Brain Res. 1619 (2015) 1–11, https://doi.org/10.1016/j.brainres.2014.12.045.
[12] G. Wu, J. Zhang, Q. Zhao, W. Zhuang, J. Ding, C. Zhang, H. Gao, D.W. Pang, K. Pu, H.Y. Xie, Molecularly engineered macrophage-derived exosomes with inflammation tropism and intrinsic heme biosynthesis for atherosclerosis treatment, Angew Chem. Int. Ed. Engl. 59 (10) (2020) 4068–4074, https://doi.org/10.1002/anie.201913700.
[13] H. Kim, S.Y. Wang, G. Kwak, Y. Yang, I.C. Kwon, S.H. Kim, Exosome-guided phenotypic switch of M1 to M2 macrophages for cutaneous wound healing, Adv. Sci. 6 (20) (2019), 1900513, https://doi.org/10.1002/advs.201900513.
[14] R. Toghiani, S.S. Abolmaali, H. Najafi, A.M. Tamaddon, Bioengineering exosomes for treatment of organ ischemia-reperfusion injury, Life Sci. 302 (2022), 120654, https://doi.org/10.1016/j.lfs.2022.120654.
[15] Y. Zhu, B. Kong, R. Liu, Y. Zhao, Developing biomedical engineering technologies for reproductive medicine, Smart Medicine 1 (1) (2022), e20220006, https://doi.org/10.1002/SMMD.20220006.
[16] Z. Fu, Y. Zhuang, J. Cui, R. Sheng, H. Tomás, J. Rodrigues, B. Zhao, X. Wang, K. Lin, Development and challenges of cells- and materials-based tooth regeneration, Engineered Regeneration 3 (2) (2022) 163–181, https://doi.org/10.1016/j.engreg.2022.04.003.
[17] X. He, L. Dai, L. Ye, X. Sun, O. Enoch, R. Hu, X. Zan, F. Lin, J. Shen, A vehicle-free antimicrobial polymer hybrid gold nanoparticle as synergistically therapeutic platforms for Staphylococcus aureus infected wound healing, Adv. Sci. 9 (14) (2022), 2105223, https://doi.org/10.1002/advs.202105223.
[18] X. He, J.-T. Hou, X. Sun, P. Jangili, J. An, Y. Qian, J.S. Kim, J. Shen, NIR-II photo-amplified sonodynamic therapy using sodium molybdenum bronze nanoplatform against subcutaneous Staphylococcus aureus infection, Adv. Funct. Mater. 32 (38) (2022), 2203964, https://doi.org/10.1002/adfm.202203964.
[19] Y. Qian, Y. Zheng, J. Jin, X. Wu, K. Xu, M. Dai, Q. Niu, H. Zheng, X. He, J. Shen, Immunoregulation in diabetic wound repair with a photoenhanced glycyrrhizic

acid hydrogel scaffold, Adv. Mater. 34 (29) (2022), 2200521, https://doi.org/10.1002/adma.202200521.
[20] Z. Luo, J. Che, L. Sun, L. Yang, Y. Zu, H. Wang, Y. Zhao, Microfluidic electrospray photo-crosslinkable κ-Carrageenan microparticles for wound healing, Engineered Regeneration 2 (2021) 257–262, https://doi.org/10.1016/j.engreg.2021.10.002.
[21] Y. Gao, Q. Ma, Bacterial infection microenvironment-responsive porous microspheres by microfluidics for promoting anti-infective therapy, Smart Medicine 1 (1) (2022), e20220012, https://doi.org/10.1002/SMMD.20220012.
[22] W. Zhu, J. Mei, X. Zhang, J. Zhou, D. Xu, Z. Su, S. Fang, J. Wang, X. Zhang, C. Zhu, Photothermal nanozyme-based microneedle patch against refractory bacterial biofilm infection via iron-actuated janus ion therapy, Adv. Mater. 34 (51) (2022), e2207961, https://doi.org/10.1002/adma.202207961.
[23] B.Z. Chen, Z.Q. Zhao, M.A. Shahbazi, X.D. Guo, Microneedle-based technology for cell therapy: current status and future directions, Nanoscale Horiz 7 (7) (2022) 715–728, https://doi.org/10.1039/d2nh00188h.
[24] S.P. Sullivan, D.G. Koutsonanos, M. del Pilar Martin, J.W. Lee, V. Zarnitsyn, S.-O. Choi, N. Murthy, R.W. Compans, I. Skountzou, M.R. Prausnitz, Dissolving polymer microneedle patches for influenza vaccination, Nat. Med. 16 (8) (2010) 915–920, https://doi.org/10.1038/nm.2182.
[25] W. Ma, X. Zhang, Y. Liu, L. Fan, J. Gan, W. Liu, Y. Zhao, L. Sun, Polydopamine decorated microneedles with Fe-MSC-Derived nanovesicles encapsulation for wound healing, Adv. Sci. 9 (13) (2022), e2103317, https://doi.org/10.1002/advs.202103317.
[26] S. Li, Y. Li, F. Yu, N. Li, C. Liu, J. Mao, H. Sun, Y. Hu, Y. Zhu, M. Zhou, L. Ding, Human endometrium-derived adventitial cell spheroid-loaded antimicrobial microneedles for uterine regeneration, Small 18 (31) (2022), e2201225, https://doi.org/10.1002/smll.202201225.
[27] A. Liu, Q. Wang, Z. Zhao, R. Wu, M. Wang, J. Li, K. Sun, Z. Sun, Z. Lv, J. Xu, H. Jiang, M. Wan, D. Shi, C. Mao, Nitric oxide nanomotor driving exosomes-loaded microneedles for achilles tendinopathy healing, ACS Nano 15 (8) (2021) 13339–13350, https://doi.org/10.1021/acsnano.1c03177.
[28] Z. Wang, F. Qi, H. Luo, G. Xu, D. Wang, Inflammatory microenvironment of skin wounds, Front. Immunol. 13 (2022), 789274, https://doi.org/10.3389/fimmu.2022.789274.
[29] T. Marzo, D. La Mendola, The effects on angiogenesis of relevant inorganic chemotherapeutics, Curr. Top. Med. Chem. 21 (1) (2021) 73–86, https://doi.org/10.2174/1568026620666201126163436.
[30] M. Godoy-Gallardo, U. Eckhard, L.M. Delgado, Y.J.D. de Roo Puente, M. Hoyos-Nogués, F.J. Gil, R.A. Perez, Antibacterial approaches in tissue engineering using metal ions and nanoparticles: from mechanisms to applications, Bioact. Mater. 6 (12) (2021) 4470–4490, https://doi.org/10.1016/j.bioactmat.2021.04.033.
[31] Z. Luo, W. Peng, Y. Xu, Y. Xie, Y. Liu, H. Lu, Y. Cao, J. Hu, Exosomal OTULIN from M2 macrophages promotes the recovery of spinal cord injuries via stimulating Wnt/β-catenin pathway-mediated vascular regeneration, Acta Biomater. 136 (2021) 519–532, https://doi.org/10.1016/j.actbio.2021.09.026.
[32] L. Sheng, Z. Zhang, Y. Zhang, E. Wang, B. Ma, Q. Xu, L. Ma, M. Zhang, G. Pei, J. Chang, A novel "hot spring"-mimetic hydrogel with excellent angiogenic properties for chronic wound healing, Biomaterials 264 (2021), 120414, https://doi.org/10.1016/j.biomaterials.2020.120414.
[33] Q. Xu, M. Chang, Y. Zhang, E. Wang, M. Xing, L. Gao, Z. Huan, F. Guo, J. Chang, PDA/Cu bioactive hydrogel with "hot ions effect" for inhibition of drug-resistant bacteria and enhancement of infectious skin wound healing, ACS Appl. Mater. Interfaces 12 (28) (2020) 31255–31269, https://doi.org/10.1021/acsami.0c08890.
[34] M. Sharifiaghdam, E. Shaabani, R. Faridi-Majidi, S.C. De Smedt, K. Braeckmans, J.C. Fraire, Macrophages as a therapeutic target to promote diabetic wound healing, Mol. Ther. 30 (9) (2022) 2891–2908, https://doi.org/10.1016/j.ymthe.2022.07.016.
[35] Y. Fu, L. Yang, J. Zhang, J. Hu, G. Duan, X. Liu, Y. Li, Z. Gu, Polydopamine antibacterial materials, Mater. Horiz. 8 (6) (2021) 1618–1633, https://doi.org/10.1039/d0mh01985b.
[36] S. Gnanasekar, G. Kasi, X. He, K. Zhang, L. Xu, E.T. Kang, Recent advances in engineered polymeric materials for efficient photodynamic inactivation of bacterial pathogens, Bioact. Mater. 21 (2023) 157–174, https://doi.org/10.1016/j.bioactmat.2022.08.011.
[37] A. Mantovani, S.K. Biswas, M.R. Galdiero, A. Sica, M. Locati, Macrophage plasticity and polarization in tissue repair and remodelling, J. Pathol. 229 (2) (2013) 176–185, https://doi.org/10.1002/path.4133.
[38] M. Miao, Y. Niu, T. Xie, B. Yuan, C. Qing, S. Lu, Diabetes-impaired wound healing and altered macrophage activation: a possible pathophysiologic correlation, Wound Repair Regen. 20 (2) (2012) 203–213, https://doi.org/10.1111/j.1524-475X.2012.00772.x.
[39] G. Sun, G. Li, D. Li, W. Huang, R. Zhang, H. Zhang, Y. Duan, B. Wang, hucMSC derived exosomes promote functional recovery in spinal cord injury mice via attenuating inflammation, Mater. Sci. Eng. C 89 (2018) 194–204, https://doi.org/10.1016/j.msec.2018.04.006.
[40] C.Y. Chen, S.S. Rao, L. Ren, X.K. Hu, Y.J. Tan, Y. Hu, J. Luo, Y.W. Liu, H. Yin, J. Huang, J. Cao, Z.X. Wang, Z.Z. Liu, H.M. Liu, S.Y. Tang, R. Xu, H. Xie, Exosomal DMBT1 from human urine-derived stem cells facilitates diabetic wound repair by promoting angiogenesis, Theranostics 8 (6) (2018) 1607–1623, https://doi.org/10.7150/thno.22958.
[41] J.H. Huang, H. He, Y.N. Chen, Z. Liu, M.D. Romani, Z.Y. Xu, Y. Xu, F.Y. Lin, Exosomes derived from M2 macrophages improve angiogenesis and functional recovery after spinal cord injury through HIF-1α/VEGF Axis, Brain Sci. 12 (10) (2022), https://doi.org/10.3390/brainsci12101322.
[42] B. Gong, G.K. Asimakis, Z. Chen, T.B. Albrecht, P.J. Boor, T.C. Pappas, B. Bell, M. Motamedi, Whole-body hyperthermia induces up-regulation of vascular endothelial growth factor accompanied by neovascularization in cardiac tissue, Life Sci. 79 (19) (2006) 1781–1788, https://doi.org/10.1016/j.lfs.2006.06.025.
[43] D. Guo, Y. Huang, X. Jin, C. Zhang, X. Zhu, A redox-responsive, in-situ polymerized polyplatinum(IV)-Coated gold nanorod as an amplifier of tumor accumulation for enhanced thermo-chemotherapy, Biomaterials 266 (2021), 120400, https://doi.org/10.1016/j.biomaterials.2020.120400.
[44] J. Zeng, X. Geng, Y. Tang, Z.-C. Xiong, Y.-J. Zhu, X. Chen, Flexible photothermal biopaper comprising Cu2+-doped ultralong hydroxyapatite nanowires and black phosphorus nanosheets for accelerated healing of infected wound, Chem. Eng. J. 437 (2022), 135347, https://doi.org/10.1016/j.cej.2022.135347.
[45] Q. Wu, S. Xu, X. Wang, B. Jia, Y. Han, Y. Zhuang, Y. Sun, Z. Sun, Y. Guo, H. Kou, C. Ning, K. Dai, Complementary and synergistic effects on osteogenic and angiogenic properties of copper-incorporated silicocarnotite bioceramic: in vitro and in vivo studies, Biomaterials 268 (2021), 120553, https://doi.org/10.1016/j.biomaterials.2020.120553.